Impact of random packing on residence time distribution of particles in bubbling fluidized beds: Part 1–cross-current flow reactors

Chemical Engineering Science 302 (2025) 120724

Contents lists available at ScienceDirect

Chemical Engineering Science

journal homepage: www.elsevier.com/locate/ces

Impact of random packing on residence time distribution of particles in bubbling fluidized beds: Part 1–cross-current flow reactors

Nasrin Nemati [a,*], Tobias Pröll [b], Tobias Mattisson [a], Magnus Rydén [a]

[a] Division of Energy Technology, Department of Space, Earth and Environment, Chalmers University of Technology, Göteborg, Sweden
[b] University of Natural Resources and Life Sciences, Institute for Chemical and Energy Engineering, Vienna, Austria

ARTICLE INFO

Keywords:
Bubbling Fluidized Bed
Cross-Current Flow
Confined Fluidization
Packed-Fluidized Bed
Residence Time Distribution
Magnetic Solids Tracer

ABSTRACT

In this work, the influence of employing random packings on the residence time distribution in a bubbling fluidized bed is investigated. The bubbling fluidized bed cold-flow reactor setup allows for continuous cross-current flow of particles. Expanded clay aggregate (ECA) is employed in the packed-fluidized bed experiments as the packing. The effects of different parameters such as packing type (ECA or no packing), Fluidization number (4.4, 6.6, and 8.8), and solid throughflow rates (92, 133, and 164 g/s) are investigated. The axial dispersion and tank-in-series models are used to categorize flow patterns of particles in the packed-fluidized beds and compared to beds using no packing. Results show that the vessel's dispersion number for solids decreases in the presence of ECA packings up to fourfold compared to unpacked beds. Furthermore, tank-in-series model shows that the number of tanks for experiments utilizing packing increases by up to threefold compared to unpacked beds. The experimental results are also compared to a model known as a hybrid model. The hybrid model considers a continuous-stirred-tank-reactor in series with a plug-flow-reactor. Comparison of the model to the measured data shows a clear shift of the relative size or residence time from the stirred tank reactor towards the plug flow reactor with axial dispersion in the packed-fluidized bed compared to a bed with no packing. Also the vessel dispersion number of the plug flow reactor model with axial dispersion is significantly decreased in the case of packed-fluidized bed.

1. Introduction

In chemical engineering, plug flow reactors (PFR) and continuous stirred tank reactors (CSTR) represent two distinct ideal steady-state flow reactor configurations. In PFR, the defining characteristic is the orderly flow of fluid through the reactor, devoid of any overtaking or mixing between fluid elements ahead or behind the average fluid front. While lateral mixing may occur within a PFR, no mixing or diffusion must occur along the longitudinal flow path. The essential condition for achieving plug flow is uniform residence time for all fluid elements (Levenspiel, 1999; Levenspiel, 2012). In contrast, CSTR maintains a state of thorough stirring, ensuring the composition of the exit stream from this reactor mirrors that of the fluid within any part of the tank (Levenspiel, 1999; Levenspiel, 2012). Real-world reactors, however, deviate from these idealized cases, necessitating investigation into parameters like the residence time distribution (RTD) for valuable insights (Levenspiel, 1999; Levenspiel, 2012; Fogler, 1999).

Gao et al. (Gao et al., 2012) summarized the application of RTD in various processes that utilize solids, including continuous blender, extruder, rotary drum, and fluidized beds (FB). Publications on FBs have often focused on circulating fluidized beds (CFB), resembling batch reactors, with the riser section conceptualized as a continuous flow reactor (Gao et al., 2012). Different methods have been employed to determine RTD of solids in CFB, with Harris et al. (Harris et al., 2002; Harris et al., 2003) providing a comprehensive evaluation of the relative merits of these techniques. The methodologies include the use of radioactive tracers (Helmrich et al., 1986; Hull and Rosenberg, 1960), colored (Kojima et al., 1989), ferromagnetic (Yerushalmi, 1985), phosphorescent substances (Wei et al., 1995; Wei and Zhu, 1996) as well as tracers of varying temperature or particle size (Smolders and Baeyens, 2000; Wei et al., 1993), etc. The radioactive tracers had been used primarily in studies. However, concerns arose regarding the elevated health risks associated with these substances. Moreover, the need for careful disposal of tracer particles at the end of experimentation had imposed significant limitations on their broader applications. On the other hand, the deployment of ferromagnetic tracer particles was deemed safe. Also, it was one of the most straightforward approaches to finding the RTD

* Corresponding author.
E-mail address: nasrinn@chalmers.se (N. Nemati).

https://doi.org/10.1016/j.ces.2024.120724
Received 25 July 2024; Received in revised form 30 August 2024; Accepted 10 September 2024
Available online 11 September 2024

Nomenclature

A	*s* (Area under the $C_{response}$ curve)
Ar	– (Archimedes number)
C	– (Normalized tracer concentration)
$C_{response}$	– (Normalized detected tracer concentration leaving the reactor)
D	m^2/s (Axial dispersion coefficient)
D/uL	– (Vessel dispersion number)
d_p	*μm* (Average particle diameter)
E	s^{-1} (Exit age distribution)
F	– (Fluidization number)
Fs	*kg/s* (Solid recirculation)
N	– (Number of tanks in series)
Pe	– (Peclet number)
t	*s* (Time)
u_{mf}	*m/s* (Minimum fluidization velocity)

Greek Letters

ρ_b	kg/m^3 (Bulk density of particles)
ρ_p	kg/m^3 (Particle density)
σ^2	s^2 (Variance of tracer curve)
σ_θ^2	– (Normalized variance of tracer curve)
$\tau_0 = 0$	s (Beginning of each experiment at which the tracer is injected into the FB.)
τ_1	s (Time lag until the detection of the tracer at the outlet coil.)
τ	s (Mean residence time of tracer in the FB.)

because of its nonreactive features (Levenspiel, 1999). Consequently, such tracers had been chosen as the preferred material for a diverse range of studies. Their distinct magnetic permeability compared to the bulk material, render them well-suited for inductive detection via coils (Guío-Pérez et al., 2013; Eder et al., 2020; Hofer et al., 2019).

In the context of bubbling fluidized bed (BFB) reactors with continuous throughflow of bed material, two situations can be expected in relation to the relative directions of the gas and solids flows: cross-current flow and counter-current flow. Investigations into particle RTD in continuous-flow BFB reactors have been limited (Hofer et al., 2019). Some researchers have proposed applying immersed baffles in the cross-current flow BFBs or changing the number of stages in the counter-current flow BFBs to manipulate the hydrodynamics of FBs and to achieve a better gas–solid contact (Eder et al., 2020; Bachmann et al., 2017; Kong et al., 2018; Zhu et al., 2020). However, the incorporation of fixed parts to the FB such as e.g. tube bundles involve several challenges including erosion, complex maintenance, and potential obstacles with mechanical stress at elevated temperatures.

An alternative method for altering the hydrodynamics in BFBs is through the implementation of the packed-fluidized bed concept, also known as confined fluidization. This concept, illustrated in Fig. 1, involves the use of inert stagnant random packings to inhibit bubble formation and bubble growth, potentially influencing hydrodynamics and RTD in BFB, which could have advantages with respect to heat and mass transfer between different phases in the bed.

Investigations into packed-fluidized beds have covered aspects such as bed expansion, pressure drop (Donsì et al., 1989; Donsì et al., 1990), determination of minimum fluidization conditions (Ziółkowski and Michalski, 1992), studying the hydrodynamics of confined fluidization employing non-spherical packing solids (Buczek and Zabierowski, 2016), and kinetics and mass transfer aspects (Farrell and Ziegler, 1979).

Recent research by Nemati et al. (Nemati and Rydén, 2021; Nemati et al., 2022; Nemati et al., 2021) explores the impact of different types of packings in BFB batch experiments, revealing that metal packings like RMSR (stainless steel thread saddle rings) and Hiflow (stainless steel pall rings) contribute to enhanced gas–solid mixing and improved fuel conversion rates compared to conventional BFB without packing in applications such as chemical-looping combustion (CLC). On the other hand, they observed that spherical packings in FBs affect solid flux due to their low void factor (Nemati et al., 2023). These observations underscore the importance of understanding the effect of packing on BFB reactor with continuous throughflow of solids and their performance. Since most of the studies on the continuous throughflows have been conducted without packings, there is a significant need for more comprehensive investigations in this area.

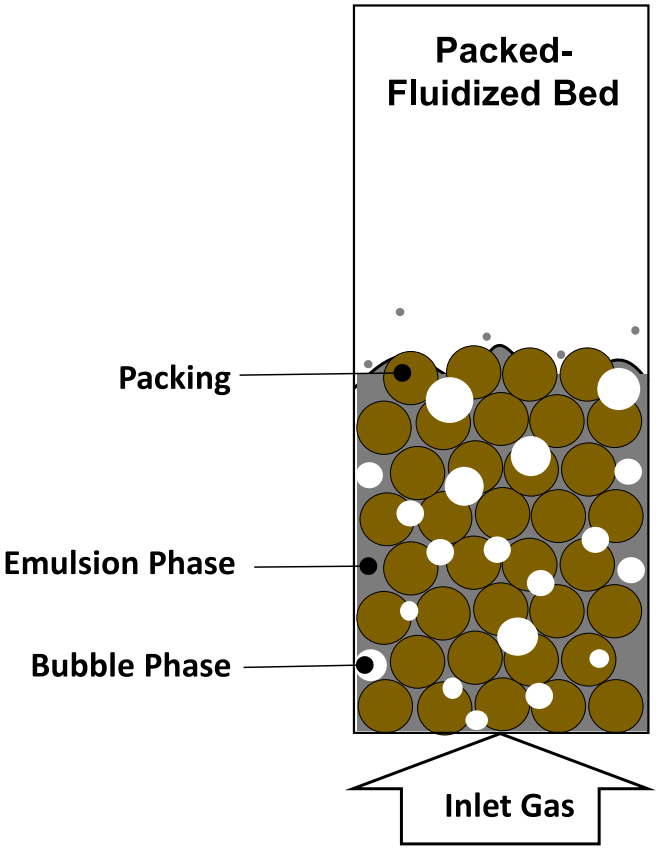

Fig. 1. Illustration of packed-fluidized bed (or confined fluidized bed).

2. Aim of this study

The main purpose of this investigation is to determine the influence of employing random packings on the solids residence time distribution and mixing characteristics in a BFB with cross-current flow of solids and gases. To fulfill this objective, experiments are conducted using a BFB setup, that allows for cross-current flow with continuous solids throughflow. The effect of different parameters such as packing type, gas velocity, and solids circulation is studied in this research.

3. Methodology

3.1. Experimental set-up

The experiments are performed in a cold-flow rectangular cuboid reactor which provided a cross-current flow of solids and gas. The experiments are conducted at room temperature and atmospheric pressure. The general setup of the reactor was previously designed and described by Hofer et al. (Hofer et al., 2019). The setup with packings applied is illustrated in Fig. 2.

The chamber of the fluidized bed has cross-sectional dimensions of 0.4 m in length and 0.2 m in width, with an overall height of the BFB reaching approximately 0.4 m. Utilizing differential pressure sensors (Kalinsky, DS2-420, 100 mbar range), the pressure drop across the entire bed height can be measured. The outlet of freeboard is equipped with an exhaust gas filter to prevent the release of fines. Gas distribution for fluidization is achieved through a 6 mm thick aluminum plate featuring 74 individual sintered metal filters. During operation, particles are continuously extracted from the outlet of the fluidized bed, recirculated, and introduced opposite the point of withdrawal, creating a net cross-current flow of gas and solids, as illustrated in Fig. 2 above. Solids circulation is generated as described below. A screw conveyor, driven by a frequency-controlled motor, provides a constant and adjustable flow of solids out of the BFB. In a small compartment at the discharge of the screw conveyor, particles are fluidized with air. Solids are then lifted in a riser with a 36 mm inner diameter (ID), connected to the compartment at the lower end. A particle separator is connected at the uppermost position of the riser. While the gaseous phase is transmitted to the freeboard, particles are directed downward, returning back into the BFB through the inlet demonstrated in Fig. 2. Further details about this configuration can be found in the works of Hofer et al. (Hofer et al., 2019; Hofer et al., 2018) and Eder et al (Eder et al., 2020).

The setup incorporates the magnetic tracer detection principle to measure particle RTDs. A custom-designed tracer detection device, inspired by the work of Guío-Pérez et al. (Guío-Pérez et al., 2013) and Hofer et al. (Hofer et al., 2019) is implemented. Inductors are employed to sense the magnetic tracer particles, causing a change in the coils' inductance as they pass through. As depicted in Fig. 2, a magnetic coil is placed at the feed side and another at the reactor's exit. The alterations in inductance are then recorded by the coils for subsequent analysis of particles RTD.

3.2. Bed material

The properties of the tracer will influence the RTD. An optimal selection of tracer and bed material would ideally involve the use of a magnetic tracer and a bed material with matching particle density, bulk density, and particle size, ensuring equivalent fluidization characteristics in a fluidized bed system. However, due to constraints encountered in this study, achieving exact equivalence in these properties is not feasible. Consequently, the chosen bulk material and tracer are selected to demonstrate as good as possible conformity in their fluid-dynamic properties, specifically ensuring similarity in the minimum fluidization velocity (u_{mf}) (Eder et al., 2020; Hofer et al., 2019). In cases where the tracer material differs in density, either being lighter or heavier, it is recommended to adjust the particle size to ensure that the u_{mf} and Archimedes number (Ar) of both materials remain closely aligned.

The characteristics of the used materials are detailed in Table 1. Both the bed material and the tracer fall under the classification of Geldart type B (Geldart, 1973). Because of the large difference in their magnetic permeability properties compared to bulk materials, steel particles are selected as the tracer used to measure particle RTDs. The material of the flow tracer is the ferritic stainless steel designated as 1.4742. The amount of tracer used in these experiments is selected based on prior studies conducted with the same coil inductors (Eder et al., 2020; Hofer et al., 2019; Eder, 2021). A consistent quantity of 0.2 kg of tracer is employed in the experiments. This amount is sufficient to ensure detection by the measurement system as the tracer passes through the magnetic coil positioned at the feed side. This quantity is chosen to generate a narrow-width signal at the setup's inlet, resembling a Dirac delta function pulse.

In Table 1, the minimum fluidization velocity, u_{mf} (m/s), is the lowest velocity of the fluidizing gas at which a bed of solid particles starts to exhibit a fluid-like behavior. At u_{mf}, the drag force exerted by the fluid on the particles balances the gravitational force acting on the particles, resulting in the fluidization of the bed. In this study, the correlation derived by Chitester et al. is applied to calculate u_{mf} (Eq. (1)) (Kunii, 1991).

Table 1
Fluidized bed material and tracer properties for cross-current flow experiments.

Reactor type		Cross-current flow	
Material		Inert	Tracer
Properties	unit	Glass bead	Ferritic stainless steel 1.4742
d_p	μm	130	72
ρ_p	kg/m^3	2450	7579
ρ_b	kg/m^3	1570	n/a
Ar	–	188	99
u_{mf}	m/s	0.017	0.016

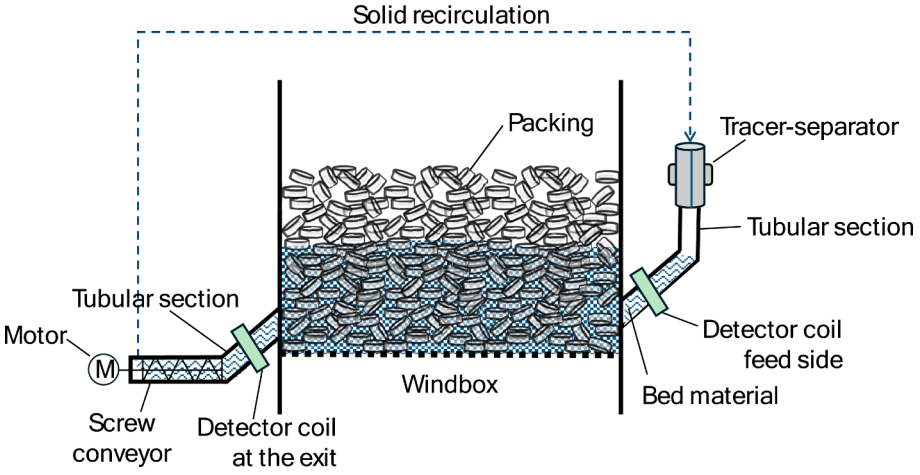

Fig. 2. The rectangular cuboid laboratory-scale cold flow model setup.

$$\frac{d_p u_{mf} \rho_g}{\mu} = \left[(28.7)^2 + 0.0494 \times Ar\right]^{1/2} - 28.7 \quad (1)$$

where, Ar (−) is the dimensionless Archimedes number and is calculated through Eq. (2).

$$Ar = \frac{d_p^3 \rho_g (\rho_s - \rho_g) g}{\mu^2} \quad (2)$$

3.3. Packing material

In this study, expanded clay aggregate (ECA) with an average diameter of 12 mm, is employed as the packing material (Fig. 3).

The selection of ECA packings as the packing material in this study is primarily driven by their semi-spherical shape and low void factor of 0.58. These characteristics mean the limited empty space between packings. Therefore, they hinder flow and fluidization in a fluidized bed, leading to altered solid flux and increased particle residence time. The selection is further supported by previous research (Nemati et al., 2023), which demonstrated the significant impact of spherical packings on system fluid dynamics due to their low void factor. Another critical factor in choosing ECA packings is their relatively low bulk density of 280 kg/m^3. In contrast, denser and truly spherical packings such as e.g. aluminum silicate balls (ASB), presented significant challenges. Preliminary experiments revealed that rigidity of of ASB packings caused substantial hinderance at the reactor's inlet, particularly due to the positioning of the entrance pipe on the lower side of the reactor (Fig. 2). To mitigate this resistance, the ASB packings would need to be placed in a cage with a few centimeters of clearance from the entrance pipe, adding unnecessary complexity to the system. In contrast, the ECA packings retain a degree of fluidity and allow for smoother entry of particles into the reactor through the inlet pipe, while at the same time constitutes a flow hindrance.

The determination of bulk density for the respective packing involves loading a container of known volume and mass with packings. The bulk density is subsequently computed by dividing the increment in mass within the container with the packings by the container's volume. The void factor of packing, representing the fraction of unoccupied space between the packing, is assessed by employing the same empty container with a predetermined volume and mass. The container is initially filled with water, and the difference in mass is recorded. Following this, the container is emptied and entirely filled with the packing. Subsequently, water is added until the container reaches full capacity, and the mass is recorded again. The void factor of the packing is calculated by dividing the masses obtained in these two measurements. Due to the low density of ECA packing and its potential for flotation upon water addition, as well as its porous nature and the capacity for water absorption within its pores, the determination of the void fraction for this packing was conducted approximately ten times. The average void factor measured for the ECA packings is 0.58 (−) and the bulk density is 280 (kg/m^3).

Fig. 3. ECA packing investigated in this work.

3.4. Experimental procedure

This study explores and compares the RTD for a pulse input of the tracer in packed-fluidized beds with that of a BFB without packing material. In the experimental setup involving packing, the reactor is initially charged with the ECA packing materials. Subsequently, an initial step involves the introduction of bulk bed material to a predetermined height within the packed zone, accompanied by the establishment of an airflow conducive to a bubbling regime within the reactor.

To realize cross-current flow with respect to gas and solids, after setting the gas flow, the recirculation of bed material was initiated and controlled through the utilization of the screw conveyor. Upon achieving a steady-state flow of material entering and leaving the reactor, a small batch (200 g) of tracer material is introduced upstream of the fluidized bed. The steady-state flow of inert material continues throughout the remaining duration of the experiments. The termination criterion for the experiment is met when there is no longer any detection of tracers in the coil positioned at the exit of the reactor.

A series of experiments is conducted, varying parameters such as packing, superficial gas velocity, and recirculation. Table 2 presents the detailed test matrix for cross-current flow experiments.

The dimensionless Fluidization number, F (−), in Table 2 represents the ratio between the superficial gas velocity and u_{mf} (m/s). As presented in Table 2, the settled bed height for all experiments was maintained at 10 cm, which is considerably lower than the packing height of 20 cm. This arrangement ensures that, at investigated fluidization conditions, the bed particles remain confined within the packed zone, preventing any migration to the region above the packed section and thus avoiding the formation of a segregated zone.

3.5. Data evaluation: Measuring RTD in FBs

The solid elements take different routes through the reactor and exhibit different durations of time to pass through the vessel. The characterization of the residence time distribution for the solid stream leaving the vessel is called the RTD of fluid or the exit age distribution E (s^{-1}) curve. The E-curve is a normalized distribution so the area beneath the curve equals unity (Levenspiel, 1999; Levenspiel, 2012).

$$\int_0^\infty \mathrm{E(t)}\,\mathrm{dt} = 1 \quad (3)$$

The zero point in the RTD analysis is from the moment the maximum peak of the tracer is detected at the detector coil located on the feed side. In this study, a pulse input of the ferromagnetic tracer to the fluidized bed is used to determine RTD. The input pulse is reasonably close to an ideal Dirac delta function, allowing to treat the signal as an ideal pulse at the input. Therefore, the E-curve can be applied directly on the

Table 2
Test matrix.

No.	Packing			Bed inventory			Air flow	
	Type	Packing void factor [-]	Packing height [cm]	Glass bead [kg]	Settled bed height [cm]	Solid throughflow (F_s) [g/s]	Superficial gas velocity [m/s]	Fluidization number (F) [-]
1	No packing	1	–	12.6	10	92	0.15	8.8
2	No packing	1	–	12.6	10	92	0.11	6.6
3	No packing	1	–	12.6	10	92	0.075	4.4
4	No packing	1	–	12.6	10	133	0.15	8.8
5	No packing	1	–	12.6	10	133	0.11	6.6
6	No packing	1	–	12.6	10	133	0.075	4.4
7	No packing	1	–	12.6	10	164	0.15	8.8
8	No packing	1	–	12.6	10	164	0.11	6.6
9	No packing	1	–	12.6	10	164	0.075	4.4
10	ECA	0.58	20	7.3	10	92	0.15	8.8
11	ECA	0.58	20	7.3	10	92	0.11	6.6
12	ECA	0.58	20	7.3	10	92	0.075	4.4
13	ECA	0.58	20	7.3	10	133	0.15	8.8
14	ECA	0.58	20	7.3	10	133	0.11	6.6
15	ECA	0.58	20	7.3	10	133	0.075	4.4
16	ECA	0.58	20	7.3	10	164	0.15	8.8
17	ECA	0.58	20	7.3	10	164	0.11	6.6
18	ECA	0.58	20	7.3	10	164	0.075	4.4

measured output without the need for numerical deconvolution of input and output signals.

The normalized detected tracer concentration leaving the reactor, $C_{response}$ (−), is used for analyses. The area, A (s), under the $C_{response}$ is calculated using Eq. (4).

$$A = \int_0^\infty C_{response,t}\,dt \cong \sum_t C_{response,t}\Delta t_i \tag{4}$$

The data obtained with the RTD measurement system was recorded every 0.035 s (Hofer et al., 2019) and used for subsequent analysis, i.e. the determination of A in Eq. (4). E-curve is determined with Eq. (5) (Levenspiel, 1999; Levenspiel, 2012).

$$E(t) = \frac{C_{response,t}}{A} \tag{5}$$

Table 3 lists parameters of FB that can be evaluated from the E-curve.

The dimensionless RTD function, E_θ, serves as a valuable metric for analyzing packed-fluidized beds. In this study, the settled bed height is maintained constant at 10 cm for both packed and unpacked beds, resulting in significantly smaller quantity of bed material in the packed cases. Consequently, the overall mean residence time of the particles changes between the studied cases, with the packed-fluidized bed cases exhibiting shorter mean residence times for the same particle inlet flow rate. The dimensionless E-curve, E_θ, plotted against dimensionless time, θ, effectively illustrates and compares the changes in the RTD patterns between packed and unpacked fluidized beds (Eqs. (6)–(8)).

Table 3
Characteristic values of the FB reactor determined from the E-curve.

Parameter	Unit	Definition
$\tau_0 = 0$	s	Beginning of each experiment at which the tracer is injected into the FB.
τ_1	s	Time lag until the detection of the tracer at the outlet coil.
τ	s	Mean residence time of tracer in the FB.

$$E_\theta(\theta) = \tau E(t) \tag{6}$$

where,

$$\theta = \frac{t}{\tau} = t\frac{\int_0^\infty C_{response,t}\,dt}{\int_0^\infty tC_{response,t}\,dt} \tag{7}$$

$$\tau = \frac{\int_0^\infty tC_{response,t}\,dt}{\int_0^\infty C_{response,t}\,dt} \tag{8}$$

4. Modeling

4.1. Dispersion and tanks-in-series models

Different models exist to categorize flow patterns based on their proximity to PFR, CSTR, or somewhere in between. The axial dispersion model and the tanks-in-series model are introduced to address deviations from plug flow in reactors. When a diffusion-like process is imposed on plug flow, it is termed axial dispersion or longitudinal dispersion. The axial dispersion coefficient, D (m^2/s), characterizes the extent of this spreading phenomenon. A higher D signifies rapid spreading of the tracer curve, while a lower D indicates slower spreading, and D=0 corresponds to no spreading, representing PFR. The dimensionless group D/uL, known as the vessel dispersion number, quantifies the spread throughout the entire vessel. Notably, D/uL and Péclet number (Pe) are inversely related (Eq. (9)).

$$Pe = \frac{uL}{D} \tag{9}$$

where, L (m) is the characteristic length, representing the distance between the two designated measurement locations positioned at the entrance and exit of the fluidized bed (FB). Meanwhile, u (m/s) is the mean solid throughflow velocity traveling between these two measurement points.

Understanding the Pe number's definition reveals that a high Pe ($\gg$1)

in a reactor brings it closer to PFR behavior, while values ≪1 resemble patterns closer to a CSTR.

Evaluating *Pe* or *D/uL* involves examining the variance of the tracer outlet concentration curve, σ^2 (s^2). Namely, considering a plug flow outside the vessel up to the boundaries (so-called closed boundary condition), the relationship between the variance of the tracer outlet concentration and *D/uL* can be expressed as follows for *D/uL* within the range of 0.01–1 (Levenspiel, 1999).

$$\sigma_\theta^2 = \frac{\sigma^2}{\tau^2} = 2\left(\frac{D}{uL}\right) - 2\left(\frac{D}{uL}\right)^2\left[1 - e^{-\frac{uL}{D}}\right] \qquad 0.01 < \frac{D}{uL} < 1 \tag{10}$$

The variance of the tracer outlet concentration, σ^2 (s^2), is a measure of the spread of the solids between the measurements at the inlet and outlet of the vessel and is calculated as (Levenspiel, 1999):

$$\sigma^2 = \frac{\int_0^\infty (t-\tau)^2 C_{response,t}\,dt}{\int_0^\infty C_{response,t}\,dt} = \frac{\int_0^\infty t^2 C_{response,t}\,dt}{\int_0^\infty C_{response,t}\,dt} - \tau^2 \tag{11}$$

The tank-in-series model is simple and can be used with any kinetics and flow pattern. In this model, it is assumed a number of tanks of the same size are connected in series. Each of these tanks is considered an ideal CSTR unit and represents a distinct portion or segment of the reactor. The number of tanks-in-series can be calculated in different ways. In the present study, the variance of the tracer curve, $\sigma_\theta^2(-)$, is employed to extract the information about the quantity of tanks, *N* (−), as:

$$\sigma_\theta^2 = \frac{1}{N} \tag{12}$$

In the tank-in-series model, despite achieving complete mixing within each tank, there is no mixing between the tanks, with the flow progressing sequentially from one tank to the next. This stepwise drop in concentration between each reactor suggests that the larger the *N*, the closer the behavior of the system approaches PFR.

4.2. Hybrid plug-mixed model

In this investigation, an assumption is posited regarding the existence of plug flow at the entrance and exit of the vessels (extending up to the boundaries). This assumption stems from the configuration of experimental reactors. Given the small diameter of the inlet and outlet pipes connected to the reactors, the mixing of bed materials within these regions is constrained. Consequently, the flow maintains a plug flow characteristic as it traverses these boundaries, referred to as a closed boundary condition or a closed vessel configuration (Fig. 4).

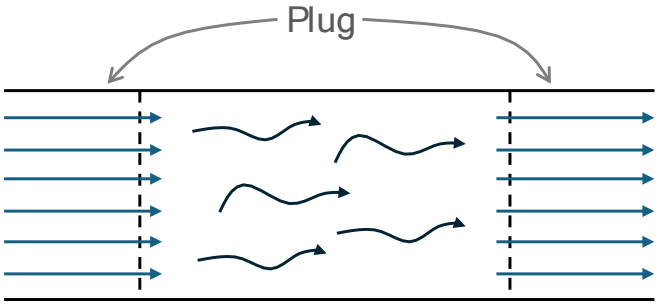

Fig. 4. Vessel with closed boundary condition.

This assumption suggests the potential adoption of a hybrid plug-mixed model for the investigated FBs in this work. This model is considered based on the position of detection coils which are placed on the sections with a PFR behavior. It entails envisioning a sequence comprising a PFR succeeded by a CSTR, followed by another PFR. To enhance model simplicity, this configuration is condensed into a simplified representation featuring two reactors in series – a CSTR and a PFR, as illustrated in Fig. 5.

The E_{hybrid}-curve is modeled for the PFR with the axial dispersion number of $\frac{D_P}{uL}$ (−) and mean residence time of τ_{PFR} (s), in series with a CSTR with mean residence time of τ_{CSTR} (s) through Eq. (13) (Eder et al., 2020; Hofer et al., 2019).

$$E_{hybrid} = E_{CSTR} \times E_{PFR} = \int_0^\infty [E_{CSTR}(t')E_{PFR}(t-t')]dt' = \frac{\sqrt{D_P}\sqrt{L}}{2\tau_{CSTR}u^{3/2}} exp\left[\frac{D_P L + \tau_{CSTR}u^2(L-ut)}{\tau_{CSTR}^2 u^3}\right]\sqrt{\frac{u^3}{D_P L}} erf\left[\frac{2D_P L + \tau_{CSTR}u^2(L+t'u-ut)}{2\sqrt{D_P}\sqrt{L}\,\tau_{CSTR}u^{3/2}}\right]_0^\infty \tag{13}$$

where,

$$E_{CSTR} = \frac{1}{\tau_{CSTR}} e^{-\frac{t}{\tau_{CSTR}}} \tag{14}$$

$$E_{PFR} = \sqrt{\frac{u^3}{4\pi D_P L}} exp\left[-\frac{(L-ut)^2}{4D_P\frac{L}{u}}\right] \tag{15}$$

The mean residence time based on the hybrid model can be calculated as:

$$\tau_{model} = \int_0^\infty t E_{hybrid}\,dt = \tau_{CSTR} + \tau_{PFR} \tag{16}$$

The validity of the model is evaluated by means of correlation coefficient R^2.

5. Results

In this investigation, a nonreactive tracer was introduced into the system via a pulse input method to examine the E-curve. Section 5 provides the results regarding the reactor behavior that can be derived from the analysis of the E-curve data.

5.1. Solids RTD curves

Fig. 6 illustrates the E-curve over time in cross-current flow experiments conducted at a solid circulation rate of 164 g/s and F=4.4. The experiments encompass two scenarios: one involving a bed with ECA and the other without packing.

Fig. 6a shows that the input pulse approximates an ideal Dirac pulse closely enough to validate the assumption of an ideal pulse at the inlet. Consequently, RTD Function can be applied directly to the measured

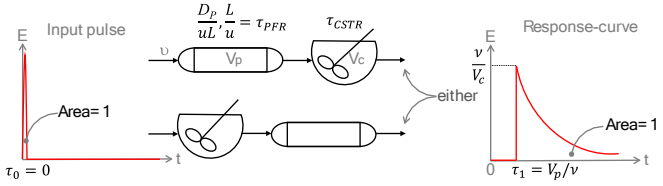

Fig. 5. Configuration of hybrid plug-mixed reactors.

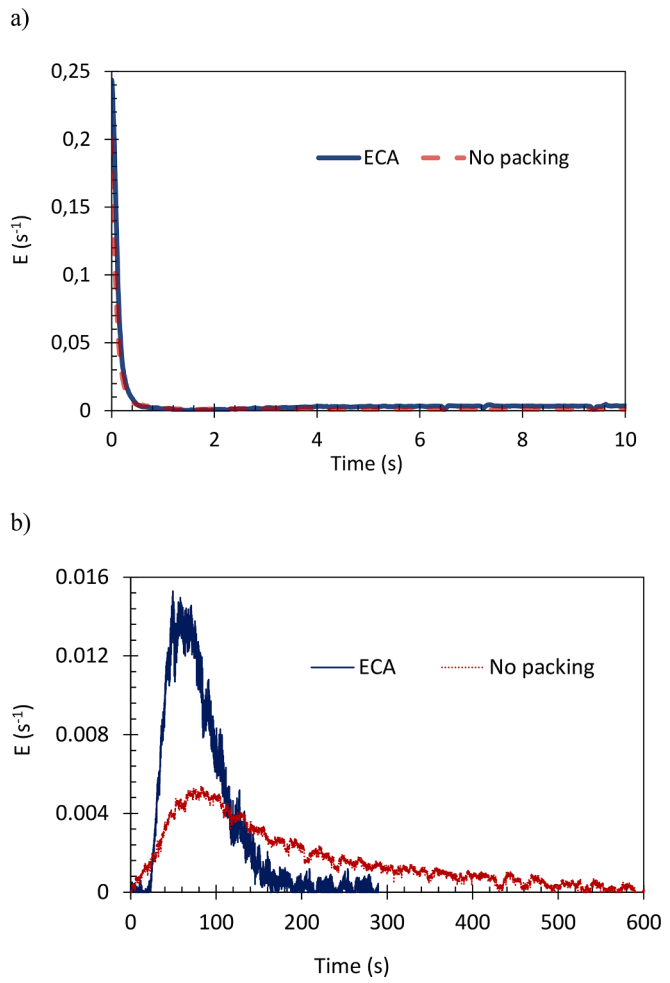

Fig. 6. E-curve for the cross-current flow BFB as a function of time, solid throughflow Fs = 164 g/s, fluidization number F=4.4: a) at the inlet, b) at the outlet.

output signal without necessitating numerical deconvolution of the input and output signals. It is evident in Fig. 6a and Fig. 6b that the duration of the input pulse is negligible relative to the duration of the response. As depicted in Fig. 6b, the incorporation of ECA packing within the BFB system significantly influences the particle behavior and RTD within the bed. In the bed without packing, tracer detection at the reactor outlet commences shortly after the injection of the pulse into the system, approximately at $\tau_1 = 9$ s (t = 0 s represents the onset of pulse injection). The concentration profile within the unpacked bed reaches its peak around 74 s, gradually diminishing over a span of approximately 600 s until complete tracer evacuation from the reactor.

In contrast, when ECA packing is introduced into the reactor, the tracer traverses the reactor length and reaches the outlet in approximately $\tau_1 = 22$ s. Subsequently, a substantial number of tracers emerge at the outlet within approximately 38 s. The peak concentration is observed at around 60 s, and by approximately 200 s, all concentration of the tracer particles has exited the reactor.

Comparative analysis of the plots representing beds with and without packing in Fig. 6b reveals that the inclusion of packing material a significant degree inhibits horizontal particle mixing in the reactor, resulting in a behavior more alike to that of a PFR with axial dispersion. This will result in the orderly flow of solids through the reactor length. Consequently, mixing or diffusion along the longitudinal flow path decreases significantly which results in an increase in τ_1, as shown in Fig. 6b. Conversely, the absence of packing material in the system aligns its behavior more closely with that of a CSTR. In this case, thorough

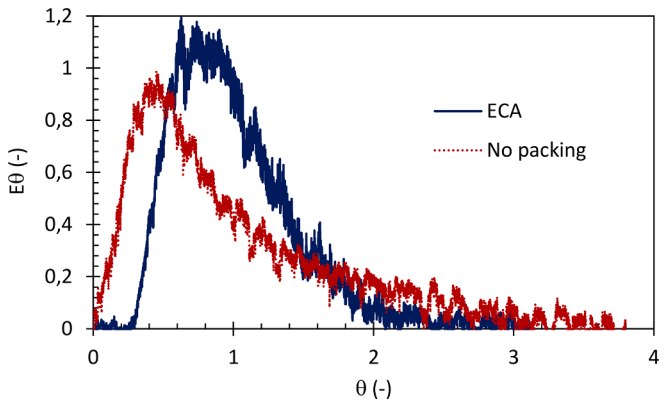

Fig. 7. E_θ-curve at the outlet of cross-current flow BFB as a function of θ, solid throughflow Fs = 164 g/s, fluidization number F=4.4.

mixing is maintained, causing the exit stream composition to reflect the solid concentration throughout the system. This thorough mixing leads to a significant decrease in τ_1, as illustrated in Fig. 6b.

It is also visible in Fig. 6b that the mean residence time is reduced in the packed bed as there is less bed material present. In order to compare the relative shape of the RTD curve between the two cases, the effect of the total inventory on the results should disappear. As described in section 3, the dimensionless E_θ function is an important tool for assessing the cases with different overall mean residence time of the particles in the bed. Fig. 7 depicts the E_θ-curve as a function of dimensionless time, θ, for the beds with and without packing.

Fig. 7 demonstrates that the incorporation of ECA packings narrows the E_θ-curve and shifts its peak towards $\theta = 1$. This indicates that the mean of the data aligns the mode, suggesting a more symmetric distribution. This indicates that the packings reduce horizontal particle mixing in the bed, resulting in a behavior that more closely resembles that of a PFR with axial dispersion. In contrast, the absence of packing material in the system results in behavior that more closely approximates that of a CSTR (Further information about E and E_θ-curve of other

Table 4
Mean residence time (τ) and time lag until the detection of the tracer (τ_1) for different Fs (g/s).

No.	Packing	Air flow	E-curve results	
	Type	F [-]	τ [s] (variation %)	τ_1 [s] (variation %)
	F_s = 92 g/s			
1	No packing	8.8	285.84 (–)	9.41 (–)
2	No packing	6.6	263.74 (–)	10.81 (–)
3	No packing	4.4	267.77 (–)	15.32 (–)
4	ECA	8.8	179.80 (−37.10)	24.70 (+162.51)
5	ECA	6.6	172.99 (−34.41)	37.28 (+244.81)
6	ECA	4.4	166.32 (−37.88)	29.40 (+91.87)
	F_s = 133 g/s			
7	No packing	8.8	243.61 (–)	10.74 (–)
8	No packing	6.6	337.62 (–)	14.00 (–)
9	No packing	4.4	262.63 (–)	17.17 (–)
10	ECA	8.8	183.06 (−24.85)	20.01 (+86.41)
11	ECA	6.6	218.48 (−35.29)	26.00 (+85.71)
12	ECA	4.4	121.26 (−53.83)	30.22 (+76.05)
	F_s = 164 g/s			
13	No packing	8.8	171.94 (–)	8.06 (–)
14	No packing	6.6	222.54 (–)	12.92 (–)
15	No packing	4.4	182.58 (–)	9.03 (–)
16	ECA	8.8	106.94 (−37.80)	19.06 (+136.37)
17	ECA	6.6	126.31 (−43.24)	26.93 (+108.42)
18	ECA	4.4	78.71 (−56.89)	22.40 (+148.21)

operating conditions can be found in Figs S1–S5 in the supplementary section).

Results of different operational conditions are compiled in Table 4, including the mean residence time of the tracer within the FB, τ, and the time interval between tracer injection at $\tau_0 = 0$ s, and the detection of the initial tracers exiting the FB at τ_1. The variation of τ and τ_1 for the packed bed compared to the unpacked bed is also presented in Table 4.

As displayed in Table 4, τ decreases in the bed containing ECA packings compared to unpacked beds at all the investigated superficial gas velocities and solid recirculation rates. This reduction reaches up to 57 % when packings are applied. This finding underscores the potential for decreasing axial dispersion within the FB through packing application, resulting in a decrease in the average residence time of particles (Further investigation into axial dispersion will be conducted in the subsequent section). Additionally, Table 4 provides data on the time lag until tracer detection, which increases by 76 % to 245 % when packings are used. This, together with the average residence time of the tracer inside the bed, suggests that the E-curve with packings approaches closer to a gaussian shape, indicating that the system behavior aligns more closely with that of a PFR.

Table 4 also presents the effect of solids throughflow, F_s, on the residence time distribution. As shown, increasing F_s at a fixed fluidization number, F, significantly amplifies the difference between the unpacked and packed beds. This is because higher F_s enhances the plug flow behavior of solids in the packed bed, while the unpacked bed continues to exhibit behavior similar to that of a CSTR. Consequently, the differences between the two cases become more pronounced at higher solids circulation rates.

5.2. The dispersion and tank-in-series model

Table 5 presents the parameters derived from cross-current flow experiments when modeled with both the dispersion and tank-in-series models. These results are summarized for different solid throughflows, F_s (g/s), fluidization number, F (−), and packing configurations.

The vessel dispersion number, D/uL (−), is the parameter that measures the extent of axial dispersion and is calculated for the experimental scenarios using Eq. (10). Subsequently, the Pe (−) is derived from Eq. (9). As depicted in Table 5, the utilization of ECA packing consistently leads to an increase in the Pe across all examined scenarios, surpassing up to fourfold the Pe value observed in unpacked beds.

On the other hand, $\sigma_\theta{}^2$ (−) is also an indicator of the dispersion of the E-curve and is calculated for different cases through Eqs (10) and (11). A lower value of $\sigma_\theta{}^2$ indicates decreased dispersion within the E-curve and lower degrees of scattering. Consequently, the reactor behavior tends towards resembling a PFR, leading to an increase in the number of theoretical tanks, N (−), required (Eq. (12)). Comparing the N values between experiments utilizing ECA packing and those conducted with an unpacked bed, it is evident that the introduction of packings results in an increase in N by up to threefold in comparison to the unpacked beds. Consequently, the reactor's behavior converges towards that of a PFR characterized by higher Pe and N values.

It is expected that the ratio of the number of tanks, N (−), between the packed and unpacked beds increases at lower fluidization numbers. As discussed in relation to Fig. 6, the unpacked bed behaves similarly to a CSTR, where N is expected to be close to 1, as shown in Table 5. In contrast, packed fluidized beds tend to exhibit PFR characteristics, with the number of tanks influenced by operating conditions such as the fluidization number. The ECA packing has lower density than the bed material and thus displays a degree of fluidity, and becomes more mobile at higher fluidization numbers, which can be expected to allow for less hindrance for cross-flow of bed material. At lower fluidization numbers, reduced bubble formation and bubble size within the bed results in significantly decreased mixing compared to higher fluidization numbers. This reduction in mixing leads to a higher number of tanks and an increased Peclet number, as reflected in Table 5.

Table 5
Parameters of dispersion and tank-in-series model for cross-current flow: for different Fs (g/s), F (−), and packing type.

No.	Packing	Air flow	Dispersion		Tank in series	
	Type	F [-]	D/uL [-]	Pe [-] (ratio)	$\sigma_\theta{}^2$[-]	N [-] (ratio)
	F_s = 92 g/s					
1	No packing	8.8	0.47	2.13 (−)	0.55	1.8 (−)
2	No packing	6.6	0.50	1.99 (−)	0.57	1.8 (−)
3	No packing	4.4	0.48	2.07 (−)	0.56	1.8 (−)
4	ECA	8.8	0.24	4.15 (2)	0.37	2.7 (1.5)
5	ECA	6.6	0.13	7.61 (3.8)	0.23	4.4 (2.4)
6	ECA	4.4	0.11	8.81 (4.3)	0.20	5.0 (2.8)
	F_s = 133 g/s					
7	No packing	8.8	0.66	1.50 (−)	0.64	1.6 (−)
8	No packing	6.6	0.48	2.06 (−)	0.56	1.8 (−)
9	No packing	4.4	0.36	2.76 (−)	0.48	2.1 (−)
10	ECA	8.8	0.23	4.31 (2.9)	0.36	2.8 (1.75)
11	ECA	6.6	0.15	6.71 (3.3)	0.25	3.9 (2.2)
12	ECA	4.4	0.12	8.08 (2.9)	0.22	4.6 (2.2)
	F_s = 164 g/s					
13	No packing	8.8	0.42	2.38 (−)	0.52	1.9 (−)
14	No packing	6.6	0.49	2.05 (−)	0.56	1.8 (−)
15	No packing	4.4	0.41	2.47 (−)	0.51	1.9 (−)
16	ECA	8.8	0.14	7.12 (3.0)	0.24	4.1 (2.2)
17	ECA	6.6	0.14	7.09 (3.5)	0.24	4.1 (2.3)
18	ECA	4.4	0.11	8.99 (3.6)	0.20	5.1 (2.7)

5.3. The E-curve for hybrid plug-mixed model

The formulation of a model incorporating a series arrangement of a PFR and a CSTR is obtained via Eq. (13) (see section 4.2). Different scenarios are explored by adjusting three independent parameters of τ_{CSTR}, D_p/uL, and τ_{PFR}. The outcomes of this model for $F_s = 164$ g/s and F=4.4 are plotted and compared with the experimental data for both packed and unpacked beds and is depicted in Fig. 8.

As seen in Fig. 8, the model demonstrated a very good fit for both cases with a coefficient of determination, R^2, equal to 0.98. Comprehensive results detailing different parameters across all investigated scenarios in the hybrid reactors model are summarized in Table 6.

Table 6 shows that for all the cases, when ECA packing is used, τ_{CSTR} and thus the size of the CSTR reactor decreases compared to the similar case without packing. On the other hand, τ_{PFR} and thus the size of the PFR reactor increases when applying packings. Furthermore, the total mean residence time based on the hybrid model, τ_{model}, aligns with the value obtained through experimental calculations, τ, providing good evidence of the predictive accuracy of the model.

In more detail, the model outcomes demonstrate notable differences in the relative share of the residence time τ in the CSTR ($\tau_{CSTR/}\ \tau_{model}$) and PFR ($\tau_{PFR/}\ \tau_{model}$) for the packed fluidized bed and the bed without packings. For the unpacked bed, the relative share of the $\tau_{PFR/}\ \tau_{model}$ is approximately 0.1. However, in the packed bed, this value increases to approximately 0.4. This observation signifies a fourfold increase in τ_{PFR} for the packed bed configuration. Additionally, the D_p/uL in the PFR for the packed bed is found to be three times smaller compared to the PFR in the unpacked bed. These findings collectively suggest that, in the context of a dual-reactor setup, the required size of the associated PFR is larger for the packed bed. Simultaneously, the degree of axial dispersion in the PFR reactor is elevated for the unpacked bed configuration. Consequently, the operational characteristics of the BFB with packing approach those of a PFR.

The validity of the model is assessed in Table 6 through R2. It is evident from Table 6 that, with the exception of two cases, R^2 exceeds 97 % for nearly all scenarios.

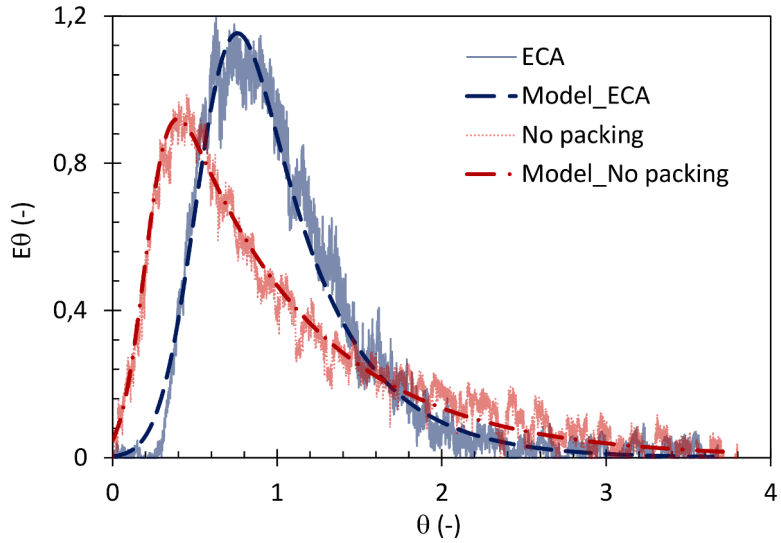

Fig. 8. Modeling results for RTD as a function of time: solid throughflow Fs = 164 g/s, fluidization number F=4.4.

Table 6
The parameters of the hybrid reactors model.

No.	Packing	Air flow	E_{hybrid}-curve model				Model validity	Experiments	Comparison
	Type	F (−)	τ_{CSTR}/τ_{model} [-]	τ_{PFR}/τ_{model} [-]	τ_{model} [s]	D_p/uL [-]	R^2	τ [s]	$\frac{\tau_{model}-\tau}{\tau}\times 100$
	F_s = 92 g/s								
1	No packing	8.8	0.93	0.07	316.12	0.14	0.97	285.84	10.6
2	No packing	6.6	0.92	0.08	282.90	0.12	0.99	263.74	7.3
3	No packing	4.4	0.84	0.16	276.17	0.13	0.99	267.77	3.1
4	ECA	8.8	0.70	0.30	187.43	0.09	0.98	179.80	4.2
5	ECA	6.6	0.59	0.41	182.87	0.07	0.97	172.99	5.7
6	ECA	4.4	0.40	0.60	166.93	0.11	0.99	166.32	0.4
	F_s = 133 g/s								
7	No packing	8.8	0.90	0.10	247.55	0.12	0.99	243.61	1.6
8	No packing	6.6	0.85	0.15	353.97	0.15	0.97	337.62	4.8
9	No packing	4.4	0.80	0.20	273.84	0.14	0.98	262.63	4.3
10	ECA	8.8	0.72	0.28	195.38	0.12	0.98	183.06	6.7
11	ECA	6.6	0.57	0.43	232.41	0.24	0.89	218.48	6.4
12	ECA	4.4	0.47	0.53	121.29	0.07	0.98	121.26	0.0
	F_s = 164 g/s								
13	No packing	8.8	0.86	0.14	181.42	0.15	0.99	171.94	5.5
14	No packing	6.6	0.82	0.18	227.06	0.48	0.96	222.54	2.0
15	No packing	4.4	0.81	0.19	186.78	0.17	0.98	182.58	2.3
16	ECA	8.8	0.55	0.45	111.23	0.10	0.97	106.94	4.0
17	ECA	6.6	0.63	0.37	134.59	0.06	0.97	126.31	6.6
18	ECA	4.4	0.45	0.55	79.41	0.06	0.98	78.71	0.9

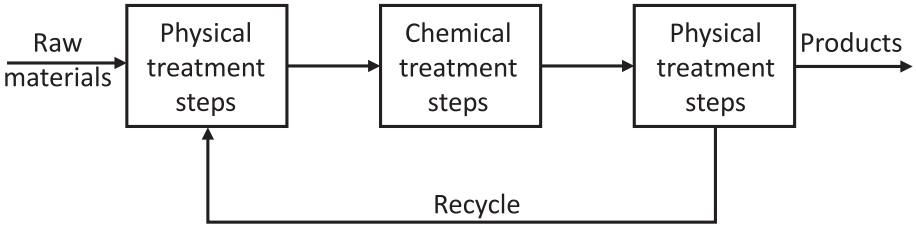

Fig. 9. An schematic diagram of a chemical process.

6. Discussion

Industrial chemical processes are typically designed to produce an economically desired product from a variety of raw materials through a series of treatment steps (Fig. 9).

Initially, raw materials pass through a number of physical treatment steps to prepare them for chemical reactions within a reactor. Subsequently, the downstream flow from the reactor undergoes further physical treatments, separations, and purifications to achieve the final desired product.

Notably, the chemical treatment step in the reactor is the heart of the process. It often determines the economic viability of the entire process.

Chemical reactions can be classified based on the phases involved, namely homogeneous and heterogeneous reactions. Numerous factors affect reaction rates, with temperature, pressure, and composition being prominent variables in homogeneous reactions. In contrast, heterogeneous reactions introduce complexities due to the fact that more than one phase is involved.

The two idealized reactors of CSTR and PFR are commonly utilized in chemical processes due to their relative simplicity and effectiveness in contacting reactants. Industrial reactor design often aims to approach these ideal reactors, or a combination thereof. A PFR facilitates a progressive decrease in reactant concentration along its length, making it more efficient for reactions where rate increases with reactant concentration, such as n^{th}-order irreversible reactions or equilibrium reactions, compared to a CSTR where concentration drops immediately to a low value.

This study investigates the impact of packings on altering the behavior of a bubbling fluidized bed (BFB) from CSTR-like to PFR-like. Experimental findings demonstrate that employing packings with low voidage, such as ECA, reduces the axial dispersion of particles in the FB, thereby approximating the behavior of a PFR.

Some example processes include steam-iron reaction (SIR), or steam methane reforming (SMR) for H_2 production (Stenberg et al., 2018; Rydén and Lyngfelt, 2006). The SIR and SMR are equilibrium reactions. Therefore, conducting these reactions in a PFR would be advantageous in shifting the equilibrium towards the products.

To elaborate on the potential applications of cross-current flow packed fluidized beds, one can consider their utility in multi-stage fluidized bed systems. Pröll et al. (Pröll et al., 2016) introduced a multi-stage, trayed two-circuit fluidized bed system designed for continuous Temperature Swing Adsorption (TSA) processes. This TSA system comprises two main columns: an adsorber and a desorber, both featuring trays to enable counter-current flow between solids and gas. In the adsorber column, CO_2 from flue gas is captured by the adsorbent through a gas–solid counterflow mechanism. Solids moved downward from the uppermost fluidized bed to the lowermost bed via downcomers, while the gas flowed upward through the fluidized beds. The CO_2-rich sorbent is then conveyed to the uppermost stage of the desorber column via a riser, where CO_2 is stripped using steam in a countercurrent fashion, exiting the column along with the steam. The lean sorbent from the desorber's lowermost stage is recirculated to the adsorber. Each stage in both columns functions as a bubbling fluidized bed (BFB). Scale-up efforts included detailed modeling and simulation to optimize the number of stages in both the adsorber and desorber, with a focus on energy efficiency. For a separation process aiming to capture 90 % of the carbon dioxide from a flue gas stream containing 10 % CO_2 by volume, a configuration with five stages in each column was proposed (Eder, 2021; Pröll et al., 2016; Pirklbauer et al., 2017). However, parameter variation studies indicated that the performance of the adsorber could be constrained by solids flow patterns and suboptimal solids residence time distribution across the stages (Eder, 2021). The cross-current packed-fluidized bed configuration presented in this work offers a potential solution to these challenges.

6.1. Limitation

A limitation of using packings in bubbling fluidized beds is the potential restriction on solids flux when low-void packings are employed, particularly where high solids circulation rates are desired, such as in circulating fluidized bed applications like chemical looping combustion (CLC). This limitation is expected, as spherical packings have a low void factor, which hinders flow and fluidization (Nemati et al., 2023).

7. Conclusion

This study explores the feasibility of enhancing the operational characteristics of a cross-current flow BFB towards a PFR through the application of packings, referred to as packed-fluidized beds or confined fluidization. The study evaluates different parameters including solid throughflows (92, 133, and 164 g/s), fluidization numbers (4.4, 6.6, and 8.8), and packing types (ECA or no packing). The key finding is that the incorporation of packing materials effectively mitigates particle mixing within the reactor. Consequently, the E-curve in the presence of packings exhibits a closer approximation to a gaussian shape, indicative of a system behavior more alike to that of a PFR. Additional conclusions drawn from this investigation are as follows:

- The utilization of ECA packing consistently results in a substantial increase in the Peclet number (*Pe*) across all investigated scenarios, exhibiting up to a fourfold increase compared to unpacked configurations.
- Analysis employing the tank-in-series model reveals a significant increase, by up to threefold, in the number of tanks (*N*) for experiments utilizing ECA packing compared to unpacked beds.
- Implementation of the hybrid plug-mixed model demonstrates for the packed-fluidized bed a shift from CSTR-like behavior toward PFR-like behavior in terms of the relative residence times in the CSTR ($\tau_{CSTR/}\ \tau_{model}$) and PFR ($\tau_{PFR/}\ \tau_{model}$).
- Furthermore, the hybrid plug-mixed model demonstrates a threefold reduction in the vessel dispersion number (D_p/uL) within the relevant PFR for the packed bed in contrast to the unpacked bed. Consequently, the level of axial dispersion in the system is much larger for the unpacked bubbling bed.

CRediT authorship contribution statement

Nasrin Nemati: Writing – review & editing, Writing – original draft, Visualization, Validation, Methodology, Investigation, Formal analysis, Data curation, Conceptualization. **Tobias Pröll:** Writing – review & editing, Validation, Resources, Methodology, Investigation, Conceptualization. **Tobias Mattisson:** Writing – review & editing, Validation, Resources, Methodology, Investigation, Conceptualization. **Magnus Rydén:** Writing – review & editing, Validation, Supervision, Resources, Project administration, Methodology, Funding acquisition, Conceptualization.

Declaration of competing interest

The authors declare that they have no known competing financial interests or personal relationships that could have appeared to influence the work reported in this paper.

Data availability

Data will be made available on request.

Acknowledgements

This work has been supported by the Swedish Energy Agency (projects 46525-1 - The application of confined fluidization in energy conversion and P2022-00544 – production of hydrogen and biochar from wood fuels with a new process that utilizes the steam-iron reaction and iron ore concentrate). Florian Pröll and Gerhard Hofer are acknowledged for valuable discussion and the support with the experiments at BOKU.

Appendix A. Supplementary data

Supplementary data to this article can be found online at https://doi.org/10.1016/j.ces.2024.120724.

References

Bachmann, P., Bück, A., Tsotsas, E., 2017. Experimental investigation and correlation of the bodenstein number in horizontal fluidized beds with internal baffles. Powder Technol 308, 378–387. https://doi.org/10.1016/j.powtec.2016.11.025.

Buczek, B., Zabierowski, P., 2016. Confined fluidization of fines in fixed bed of coarse particles. Chem. Process Eng. 37 (4), 545–557. https://doi.org/10.1515/cpe-2016-0044.

Donsì, G., Ferrari, G., Formisani, B., 1989. Expansion behaviour of confined fluidized beds of fine particles. Can J Chem Eng 67 (2), 185–190. https://doi.org/10.1002/cjce.5450670204.

Donsì, G., Ferrari, G., Formisani, B., Longo, G., 1990. Confined fluidization of fine particles in a packed bed of coarse particles: model and experimental description. Powder Technol 61 (1), 75–85. https://doi.org/10.1016/0032-5910(90)80068-A.

Eder, C., 2021. Solids Mixing and Wall-to-bed Heat Transfer in Cross-flow Bubbling Fluidized Bed Reactors with Different Immersed Tube Bundles. University of Natural Resources and Life Science, Vienna.

Eder, C., Hofer, G., Beer, J., Pröll, T., 2020. Particle mixing in bubbling fluidized bed reactors with immersed heat exchangers and continuous particle exchange. Ind Eng Chem Res 59 (44), 19736–19750. https://doi.org/10.1021/acs.iecr.0c03568.

Farrell, R.J., Ziegler, E.N., 1979. Kinetics and mass transfer in a fluidized packed-bed: catalytic hydrogenation of ethylene. AIChE J. 25 (3), 447–455. https://doi.org/10.1002/aic.690250309.

Fogler, H.S., 1999. *Elements of Chemical Reaction Engineering*; Upper Saddle River. Prentice Hall PTR, N.J.

Gao, Y., Muzzio, F.J., Ierapetritou, M.G., 2012. A review of the residence time distribution (RTD) applications in solid unit operations. Powder Technol 228, 416–423. https://doi.org/10.1016/j.powtec.2012.05.060.

Geldart, D., 1973. Types of gas fluidization. Powder Technol 7 (5), 285–292. https://doi.org/10.1016/0032-5910(73)80037-3.

Guío-Pérez, D.C., Pröll, T., Wassermann, J., Hofbauer, H., 2013. Design of an inductance measurement system for determination of particle residence time in a dual circulating fluidized bed cold flow model. Ind Eng Chem Res 52 (31), 10732–10740. https://doi.org/10.1021/ie400211h.

Harris, A.T., Davidson, J.F., Thorpe, R.B., 2002. A novel method for measuring the residence time distribution in short time scale particulate systems. Chem. Eng. J. 89 (1–3), 127–142. https://doi.org/10.1016/S1385-8947(02)00004-9.

Harris, A.T., Davidson, J.F., Thorpe, R.B., 2003. Particle residence time distributions in circulating fluidised beds. Chem Eng Sci 58 (11), 2181–2202. https://doi.org/10.1016/S0009-2509(03)00082-4.

Helmrich, H., Schügerl, K., Janssen, K., 1986. Decomposition oF NaHCO3 in Laboratory and Bench Scale Circulating Fluidized Bed Reactors. In: Circulating Fluidized Bed Technology. Elsevier, pp. 161–166. https://doi.org/10.1016/B978-0-08-031869-1.50019-3.

Hofer, G., Schöny, G., Pröll, T., 2018. Acting on hydrodynamics to improve the local bed-to-wall heat transfer in bubbling fluidized beds. Chem. Eng. Res. Design 134, 309–318. https://doi.org/10.1016/j.cherd.2018.04.015.

Hofer, G., Märzinger, T., Eder, C., Pröll, F., Pröll, T., 2019. Particle mixing in bubbling fluidized bed reactors with continuous particle exchange. Chem Eng Sci 195, 585–597. https://doi.org/10.1016/j.ces.2018.10.001.

Hull, R.L., Rosenberg, AE.V., 1960. Radiochemical tracing of fluid catalyst flow. Ind Eng Chem 52 (12), 989–992.

Kojima, T., Ishihara, K., Guilin, Y., et al., 1989. Measurement of solids behaviour in a fast fluidized bed. J. Chem. Eng. Japan 22 (4), 341–346.

Kong, W., Wang, B., Baeyens, J., Li, S., Ke, H., Tan, T., Zhang, H., 2018. Solids mixing in a shallow cross-flow bubbling fluidized bed. Chem Eng Sci 187, 213–222. https://doi.org/10.1016/j.ces.2018.04.073.

Kunii, D. O.; Levenspiel. *Fluidization Engineering*, 2nd ed.; Brenner, H., Ed.; Butterworth-Heinemann: Newton, MA, USA, 1991.

Levenspiel, O., 2012. Tracer Technology Vol. 96. https://doi.org/10.1007/978-1-4419-8074-8.

Levenspiel, O. *Chemical Reaction Engineering*; 1999; Vol. 38.

Nemati, N., Andersson, P., Stenberg, V., Rydén, M., 2021. Experimental investigation of the effect of random packings on heat transfer and particle segregation in packed-fluidized bed. Ind Eng Chem Res 60 (28), 10365–10375. https://doi.org/10.1021/acs.iecr.1c01221.

Nemati, N., Filiu Moreno, P., Rydén, M., 2023. Investigation of the hydrodynamics of packed-fluidized beds: characterization of solids flux. Fuel 335, 127010. https://doi.org/10.1016/j.fuel.2022.127010.

Nemati, N., Rydén, M., 2021. Chemical-looping combustion in packed-fluidized beds: experiments with random packings in bubbling bed. Fuel Process. Technol. 222, 106978. https://doi.org/10.1016/j.fuproc.2021.106978.

Nemati, N., Tsuji, Y., Mattisson, T., Rydén, M., 2022. Chemical looping combustion in a packed fluidized bed reactor—fundamental modeling and batch experiments with random metal packings. Energy & Fuels. https://doi.org/10.1021/acs.energyfuels.2c00527.

Pirklbauer, J., Schöny, G., Zerobin, F., Pröll, T., Hofbauer, H., 2017. Optimization of stage numbers in a multistage fluidized bed temperature swing adsorption system for CO2 capture. Energy Procedia 114, 2173–2181. https://doi.org/10.1016/j.egypro.2017.03.1354.

Pröll, T., Schöny, G., Sprachmann, G., Hofbauer, H., 2016. Introduction and evaluation of a double loop staged fluidized bed system for post-combustion CO 2 capture using solid sorbents in a continuous temperature swing adsorption process. Chem Eng Sci 141, 166–174. https://doi.org/10.1016/j.ces.2015.11.005.

Rydén, M., Lyngfelt, A., 2006. Using steam reforming to produce hydrogen with carbon dioxide capture by chemical-looping combustion. Int J Hydrogen Energy 31 (10), 1271–1283. https://doi.org/10.1016/j.ijhydene.2005.12.003.

Smolders, K., Baeyens, J., 2000. Overall solids movement and solids residence time distribution in a CFB-Riser. Chem Eng Sci 55 (19), 4101–4116. https://doi.org/10.1016/S0009-2509(00)00084-1.

Stenberg, V., Rydén, M., Mattisson, T., Lyngfelt, A., 2018. Exploring novel hydrogen production processes by integration of steam methane reforming with chemical-looping combustion (CLC-SMR) and oxygen carrier aided combustion (OCAC-SMR). Int. J. Greenhouse Gas Control 74, 28–39. https://doi.org/10.1016/j.ijggc.2018.01.008.

Wei, F., Lin, S., Yang, G., 1993. Gas and solids mixing in a commercial FCC regenerator. Chem Eng Technol 16 (2), 109–113. https://doi.org/10.1002/ceat.270160207.

Wei, F., Jin, Y., Yu, Z., Chen, W., Mori, S., 1995. Lateral and axial mixing of the dispersed particles in CFB. J. Chem. Eng. Japan 28 (5), 506–510. https://doi.org/10.1252/jcej.28.506.

Wei, F., Zhu, J.-X., 1996. Effect of flow direction on axial solid dispersion in gas—solids cocurrent upflow and downflow systems. Chem. Eng. J. Biochem. Eng. J. 64 (3), 345–352. https://doi.org/10.1016/S0923-0467(96)85016-0.

Yerushalmi, J., 1985. High velocity fluidization. Fluidization 225–289.

Zhu, X., Feng, X., Zou, Y., Shen, L., 2020. Effect of baffles on bubble behavior in a bubbling fluidized bed for chemical looping processes. Particuology 53, 154–167. https://doi.org/10.1016/j.partic.2020.04.003.

Ziółkowski, D., Michalski, J., 1992. Onset of fluidization of fines in an organized system within voids of packings formed of spherical elements. Chem Eng Sci 47 (15–16), 4007–4016. https://doi.org/10.1016/0009-2509(92)85150-A.